DOI 10.5162/sensor2017/D4.3

Thin-Film Calorimeter for High-Temperature Applications: Thermodynamic Characterization on Piezoelectric Langasite Temperature Sensors

Alexander Omelcenko, Hendrik Wulfmeier, Holger Fritze
Institute of Energy Research and Physical Technologies, Clausthal University of Technology, Am Stollen 19 B, 38640 Goslar, Germany

Abstract

Thin-Film Calorimetry (TFC) is a measurement technique for in-situ analysis of thermal properties such as phase transformation temperatures and enthalpies of thin films and thin-film systems. It is applicable to metals, oxides and, for example, thin-film all-solid-state electrochemical cells. This technique takes advantage of the high temperature sensitivity of piezoelectric resonators. Here, high-temperature stable piezoelectric langasite single crystals are simultaneously operated as planar temperature sensors and substrates for the films of interest. Any generation or consumption of heat in the deposited films induces changes in the otherwise undisturbed resonance frequency. This work focuses on the thermal transport in these sensors to relate the frequency fluctuations with heat generation or consumption during phase transformations. Instead of using films with more or less unknown thermodynamic properties, well defined heat pulses are applied by resistive heating via platinum heating structures. Based on this approach, a detailed thermodynamic characterization of the TFC system is provided. The effects of short energy pulses and prolonged resistive heating is studied in vacuum and in pure Ar atmosphere. Different heat transfer processes and their timescales are identified and characterized quantitatively. The latter includes the influence of thermal convection on the heat dissipation.

Key words: calorimetry, piezoelectric sensors, thermodynamic characterization, thin films, high temperature

Introduction

The use of Lithium-ion batteries (LIB) as energy storage for electronic devices is established [1], [2]. The performance of such devices with respect to high power density and high specific energy depends on synthesis methods of the used LIB materials [3]. The fabrication methods determine the materials structure, impacting not only the overall performance but also safety and lifetime of the devices [4]. Consequently, systematic investigations of material properties such as thermodynamic and kinetic parameters e.g. phase transformation temperatures and enthalpies up to the synthesis temperature of such battery materials is demanded [5]. In biomedical applications for implantable devices miniaturized power sources are required which can be realized by e.g. all-solid-state thin-film LIB [6]. Since the thermodynamic behavior of bulk samples differs often significantly from thin films [7], [8], suited measurement techniques for thin film calorimetric investigations at high temperatures are required.

The Thin-Film Calorimeter (TFC) is a measurement system for the determination of temperature and enthalpy of phase transformations (PT) of thin films. Its suitability to provide thermodynamic data in the field of LIB materials has been demonstrated [9], [10], [11], [12]. It uses piezoelectric langasite ($La_3Ga_5SiO_{14}$, LGS) resonators which serve as planar temperature sensors. They are high-temperature stable [13], [14] and are operated in thickness shear mode at their resonance frequency (f_R). Due to the strong temperature dependence of the resonance frequency, any temperature change induced by endo- or exothermic PT directly impacts f_R which enables, in principle, the determination of the enthalpy of PT. The typical operating temperature of the TFC ranges from RT up to 1000 °C. Thin films e.g. metals, oxides and thin-film systems such as all-solid-state lithium ion batteries, can be deposited on the metal electrodes of the piezoelectric temperature sensor and investigated in the temperature range mentioned above.

High-temperature thermodynamic investigation of thin films and thin film systems by TFC is a challenging task and requires detailed understanding of the heat transfer mechanisms involved. Since the TFC approach is fairly novel, a comprehensive study and systematic characterization of the resonance frequency response to temperature changes induced by thin films is necessary.

In this work a detailed thermodynamic characterization of the measurement system is presented. The experiments include a systematic study of the heat transfer mechanisms and their timescales in Ar atmosphere and in vacuum by simulating of PT via of defined energy pulses (heating pulses). For this purpose platinum heating structures are used, which are deposited on the resonators by mesh printing. Their dimensions corresponds to that of films typically deposited on the resonators.

System Development

The TFC setup (*Fig. 1*) enables the installation of two LGS resonators in a quartz glass sample holder. They are connected by platinum wires to a network analyzer. Each of these samples has a thermocouple located about 0.5 mm beneath it. The arrangement ensures simultaneous characterization of two samples under nearly identical conditions. The

sample holder is encompassed by a glass container, which makes the system gas tight and allows for measurements in defined atmospheres such as Ar, H_2/Ar and vacuum down to 10^{-6} mbar. Just above the sample holder an oxygen sensor is connected to an oxygen pump and allows for precise control of the oxygen partial pressure (p_{O2}) in the direct vicinity of the samples. This is useful for oxygen sensitive materials. A tube furnace is used to control the temperature during measurements. Thereby, a self-constructed DC power supply minimizes electromagnetic stray fields. Temperature changes are typical done with ramps of 1–5 $Kmin^{-1}$. The temperature control accuracy for set ramps and constant temperatures shows maximum deviations from set values of ±0.05 K, only.

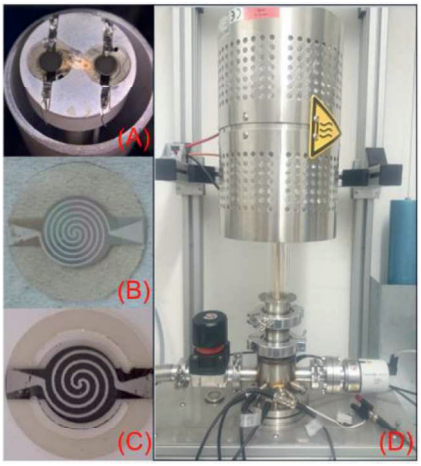

Figure 1. (A): Sample holder containing two conventional resonators; (B): conventional resonator with heating structure; (C) free standing resonator with heating structure; (D) photograph of TFC setup (furnace encloses the glass tube with the sample holder)

Measurement Principle and Data Evaluation

The TFC is based on high-temperature stable piezoelectric LGS resonators of 10 mm in diameter and 250 µm in thickness. They are coated with key-hole shaped Pt-Rh electrodes (thickness ~250 nm) on each side by pulsed laser deposition (PLD) with. While operating the devices in thickness shear mode the typical resonance frequencies (f_R) are about 5 Mhz. The temperature dependence of f_R shows continuous decrease with increasing temperature which can be approximated by a parabolic function [13]. The theoretical operation limit is the melting point at 1473 °C. Although bulk oscillations have been experimentally observed up to 1400 °C [14], the practical measurement range is limited at approximately 1000 °C due to high temperature damping. In small temperature ranges of ±10 K the temperature dependence of f_R can be approximated with a linear function to provide the temperature coefficient α_T (~100 Hz K^{-1} at 200 °C and ~400 Hz K^{-1} at 1000 °C). Thin films to be measured are typically deposited on the electrodes of the resonators or on appropriate diffusion barriers by e.g. Pulsed laser deposition (PLD), magnetron or ion beam sputtering.

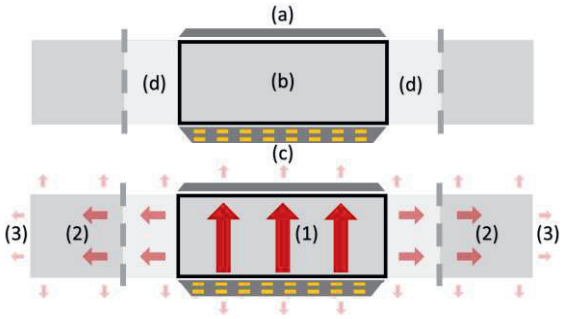

Figure 2. Scheme of resonator: (a) active material, (b) active vibrating volume, (c) heating structure, (d) removed volume in case of free-standing resonators (top); (1) heat flux into active volume, (2) heat flux into outer volume (3) heat flux into surroundings.

If the thin film of interest undergoes a phase transformation, its temperature increase differs from the undisturbed heating ramp, which is set by the furnace. Since the film is deposited on the electrode above the vibrating volume of the resonator (*Fig.2*) thermal conduction via path (1), temperature deviations of the thin film are registered as a disturbance in the otherwise continuous f_R change during heating or cooling of the resonator. An endothermic PT such as melting results in a diminished temperature increase of the vibrating volume and elevated decrease of f_R. The magnitude of the temperature change ΔT of the vibrating volume can be calculated by:

$$\Delta T_{PT} = \frac{\Delta f_R}{\alpha_T} \qquad (1)$$

Here, α_T is the temperature coefficient and Δf_R is the change in resonance frequency. They are determined from the undisturbed f_R course, just before and shortly after a PT.

The temperature shift during heat consumption or release is determined by the heat capacity C_{pres} [J K^{-1}] of the vibrating volume and can be calculated by considering all heat capacities $c_{p,i}$ and masses m_i of the components involved (resonator, electrodes, diffusion barrier, thin film of interest) for any required temperature:

$$C_{p;res(T)} = \sum_i c_{p,i;(T)} m_i \qquad (2)$$

The total quantitative heat intake or release of the vibrating resonator volume is given by ΔQ_{PT}:

$$\Delta Q_{PT} = \Delta T_{PT}\, C_{p;res} \qquad (3)$$

Finally, the enthalpy ΔH_{PT} can be calculated by:

$$\Delta H_{PT} = \frac{\Delta Q_{PT}}{m_{film}} = \frac{\Delta T_{PT}\, C_{p;res}}{m_{film}} \qquad (4)$$

Furthermore, the enthalpy can be determined by applying well defined amounts of energy via heating structures (*Fig. 1*) at temperatures which correspond to that of PT. The change in f_R directly after heat application via heating structure represents the enthalpy of a PT for identical Δf_R.

There are several heat transfer processes, which can occur when temperature changes are induced by PT of thin films or by heating structures. The related paths are depicted in *Fig. 2:*

Path 1: Heat transfer from the thin film or heating structure into the vibrating volume of the resonator

Path 2: Heat transfer from the vibrating volume of the resonator into the outer volume of the resonator

Path 3: Heat transfer from the outer resonator volume into the sample holder via thermal conduction, heat exchange of the whole resonator with the surroundings via convection and radiation (those are combined in *Fig.2*)

Induced temperature changes by heating pulses propagate to the vibrating volume of the resonator (Fig. 2 indicated conduction path (1)). The time scale of that process can be approximated with:

$$\tau \approx \frac{L^2}{4\kappa(T)} \quad (5)$$

Here, τ, κ, and L are the time constant of thermal diffusion, the thermal diffusivity and the thermal diffusion length, respectively.

The temperature increase of the vibrating resonator volume caused by a heating process is described by:

$$T(t) = \sum_i T_i (1 - exp(-t / \tau_i)) \quad (6)$$

The index *i* is used to distinguish the time constants for different heat transfer mechanism. Eq. (6) is valid for short heating pulses and for prolonged heating and used to fit the measurement data. When considering a heating process, τ and 5 τ represents the time it takes to reach 63.2% and 99.3% of the maximum value of the amplitude, respectively. In the case of overlapping heat transfer mechanisms (indicated by heat transfer paths (2), (3) in Fig.2) it may be required to fit a sum of these functions to determine the timescales of the different heat transport processes. A similar approach is required describe the cooling of the vibrating resonator volume. Here the following eq. is used:

$$T(t) = \sum_i T_i exp(-t / \tau_i) \quad (7)$$

In case of cooling τ and 5 τ represent the timescale for a temperature drop to 36.8 % and 0.7 % of the initial value, respectively. If several heat transfer mechanisms are occurring simultaneously, fitting a sum of exponential decay functions (eq. 7), may provide several time constants.

Temperature changes caused by heating pulses propagate from the heating structure into the vibrating volume of the resonator. For the heat transport perpendicular to the surface, a thermal diffusion length of L = 250 µm is assumed which corresponds to the thickness of the LGS resonators. According to eq. (5) changes of f_{R_max} should be detected after approximately $5\tau_0 \approx 0.2$ s (calculated with κ_{LGS} = 0.43 mm^2 s^{-1} at 232 °C [12]). Further, radial symmetric heat propagation into the outer resonator volume occurs. Here, the thermal diffusion length is L = 2.5 mm (indicated as thermal conduction path (2) in Fig.2). The thermal time constant for this length is calculated to be $\tau_1 \approx$ 3.8 s. This value is significantly larger than τ_0 due to the aspect ratio of the resonator of 40:1.

To simulate fast exothermic PT, short heating pulses of exactly 0.2 s are applied. Here, heat transfer mechanisms indicated by path (2) and (3) in *Fig.2* are assumed to be negligible for calculation of the enthalpy of fast PT of thin films, because of the large timescales with respect to the duration of the heat pulses and the time constant for path (1). Further, the heat dissipation curves after short heating pulses are used to determine ΔT_{max} by extrapolation of the exponential fit to the time of pulse application.

PT with large timescales require detailed, time dependent thermodynamic characterization of heat dissipation processes including paths (2) and (3) by prolonged defined heating.

In the case of vacuum, the heat transfer path (3) in *Fig.2* designates the heat conduction into the sample holder and, in principle, heat transfer due to radiation. Additionally, in presence of a gas atmosphere, heat transfer path (3) designates the heat transfer via convection, too.

Detailed analysis of the mentioned cases is presented in subsequent sections. High sensitivity of the TFC system requires to minimize the heat dissipation from the vibrating to the outer resonator volume. Therefore, free-standing resonators (FSR) are prepared and investigated. As shown in *Fig. 1*, at FSR the thermal conduction path into the outer volume is reduced which lowers the heat dissipation and increases the thermal heat transfer time for heat transfer path (2) and (3).

Resonator Preparation

Y-cut LGS resonators are purchased from SICCAS, P. R. China. The crystal boules are grown by the Czochralski method [15]. The thickness of the resonators typically varies within the range of 250–265 µm, which corresponds to thickness shear resonance frequencies of 5.0–5.4 MHz in fundamental mode. Their diameter is Ø=10 mm. These resonators are defined as conventional LGS resonators in this work. The FSR are prepared from conventional ones by removal of most of the LGS material around the vibrating volume via ultrasonic milling [16] (shown in *Fig.1).* Removal of the material reduces the thermal conduction path (2) geometrically by a factor of ~4.6. Both conventional and FSR are coated with keyhole-shaped high-temperature stable platinum-rhodium electrodes via PLD using a KrF excimer laser. Electrode thickness lies in the range of 200–300 nm with Ø=5 mm. Aluminum oxide (Al_2O_3) diffusion barriers with a thickness of 250–450 nm are deposited via PLD, too. They serve as electrical insulation for heating structures thereby ensuring good thermal conduction. On top of the diffusion barrier, platinum heating structures are deposited via mesh printing. Examples of such a heating structures are shown in Fig.1. Active materials such as Sn thin films are

deposited via PLD on the diffusion barriers. The deposition parameters are given in [9].

Devices and Parameters

The measurement of the resonance frequency f_R is performed by a network analyzer HP E5100A (USA). A measurement speed up to 150 resonance spectra per minute results in sufficient accuracy. Thermocouples Type-S in combination with a multichannel digital voltmeter Keithley DVM 2000 (USA) are used to determine the temperatures. Defined short heating pulses or prolonged heating is applied to the heating structures via a DC power supply HP 6628A (USA), which is controlled by a custom developed software for precise control of applied energy over time. Measurements in Ar atmosphere are performed applying a gas flow of 20 ml min^{-1}. Measurements in vacuum are performed at $7*10^{-3}$ mbar.

Results and Discussion

The thermodynamic characterization of conventional LGS resonators and FSR is performed in different atmospheres, i.e. vacuum and Ar. Since Sn thin films are applied to calibrate the system [10], the melting temperature of Sn (231.9 °C [17], [18]) is chosen for the investigations. After reaching stable conditions at that temperature, short energy pulses of 108 mJ are applied within 0.2 s to induce heating of the vibrating resonator volume.

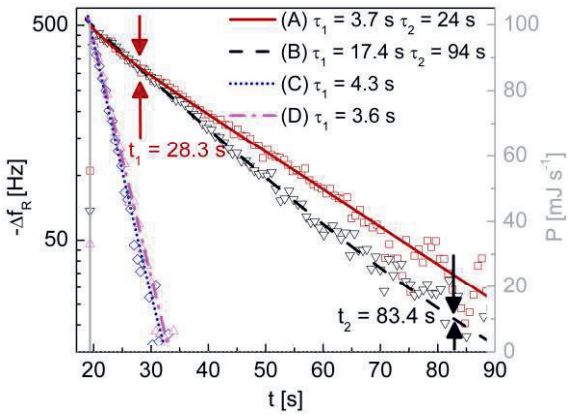

Figure 3. Logarithmic plot of the resonance frequency response of conventional resonators and FSR to short pulses of identical energy in Ar and vacuum; (A): Exp. fit conv. resonator in vacuum, (B): Exp. fit FSR in vacuum, (C): Exp. fit conv. resonator in Ar, (D): Exp. fit FSR in Ar; thermal dissipation time constants are given. P is the heating power; t_1 and t_2 mark the intersections of the two exponential fit functions used.

Fig. 3 depicts the resonance frequency course after the heating pulse application, i. e. 19 s after initiating the experiment. The heating pulse, 5 τ_0 = 0.2 s (eq. 5) causes a sudden change in f_R. The data are fitted using eq. (7). The extrapolation of the fit to the time of pulse application provides the maximum Δf_R.. Additionally, thermal dissipation time constants (τ_1, τ_2) are determined.

In *Fig. 3* no significant difference in Δf_R between Argon atmosphere and vacuum is observed for conventional resonators Δf_{R_Vac} = 501.0 Hz; Δf_{R_Ar} = 486.7 Hz. The nearly identical Δf_R response of the resonators is consistent with the assumption that the initial heat transfer from an active material or heating structure into the vibrating volume has a significantly smaller timescale than the subsequent heat dissipation processes. This observation supports the validity of the data evaluation model in [10] for fast PT of Sn.

However, there are significant differences regarding the heat dissipation processes after the initial heating of the vibrating volume. The heat dissipation in vacuum is dominated by the radial symmetric heat propagation with a time constant of τ_1 = (3.7±0.3) s. This value is close to the calculated value from eq. (5) of $\tau_1 \approx$ 3.8 s. The subsequent heat transfer processes includes heat dissipation from the resonator into the sample holder and possible radiation into the surroundings. They occur simultaneously and are not separable from each other. They are combined in the heat dissipation time constant τ_2 = (24.4±0.3 s). The radial symmetric heat dissipation and the combined dissipation into the surroundings can be identified in *Fig.3*. There, the time t_1 represents the transition between the exponential functions which is defined as intersection of the two independently regarded exponential fit functions. At this point the radial symmetric heat propagation into the outer volume of the resonator is mostly completed and the heat dissipation into the surroundings starts to dominate. In Ar atmosphere, the heat dissipation into the outer resonator volume is simultaneously overlapping with temperature exchange with the gas atmosphere (convection). The heat losses due to convection result in significantly increased heat dissipation when compared to measurements in vacuum. However, it is not possible to distinguish between the overlapping processes. Only the overall combined heat dissipation time constant of τ = (3.6±0.3 s) could be determined.

For FSR in Argon atmosphere and in vacuum Δf_R is again almost identical ($\Delta f_{R\_FSR\_Ar}$ = 511.3 Hz, $\Delta f_{R\_FSR\_Vac}$ = 532.5 Hz). These values are also similar in comparison to that of conventional resonators (identical amount of applied energy). This observation confirms that temperature changes of the vibrating volume induced by heating processes on short timescales of 0.2 s are not significantly impacted by the other dissipation processes discussed so far. The thermal heat dissipation time constant of an FSR in vacuum is determined to be τ_1 = (17.4±0.3 s) which is 4.7 times larger than for conventional resonators. This increase can be explained by the geometrical reduction of the thermal conduction path (2) of the FSR by a factor of 4.6. Heat dissipation into the surroundings is also reduced with τ_2 = (94±0.5 s). In *Fig.3* the intersection of the exponential fit functions is marked at t_2 = 83.4 s for the FSR in vacuum. In Argon atmosphere the losses due to convection are overlapping with the radial symmetric heat propagation, resulting in an overall heat dissipation time constant τ = (4.3±0.2 s). Consequently, the presence of the gas atmosphere introduces significant losses and increases heat dissipation on a large timescale, However, the maximum Δf_R is not affected if short heating pulses are applied to the heating structure. As for the conventional resonators, FSR measurements confirm, that initial heat transfer from

an active material or heating structure into the vibrating volume has a shorter time constant than the radial symmetric heat dissipation or the dissipation due to convection. Therefore, it is sufficient to use Δf_{R_max} for the determination of the enthalpy in case of fast PT.

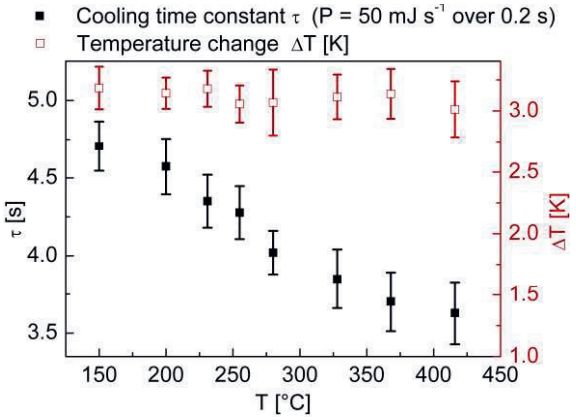

Figure 4: Temperature dependence of overall cooling time constants in Ar atmosphere (closed); Quantitative change in temperature from identical energy pulses at different temperatures (open); standard deviation error bars

Fig.4 depicts the overall cooling time constants of an FSR in Argon atmosphere ($\tau_{FSR;\ Ar}$) at different temperatures from 150 °C to 420 °C after application of a short energy pulse of 50 mJ. The corresponding temperature change ΔT of the vibrating resonator volume is also shown. A significant decrease of the overall heat dissipation time constants is observable from 150 °C to 420 °C. This suggests, that heat losses due to the heat exchange with the gas atmosphere increase with temperature. ΔT is identical at different temperatures for identical heating pulses applied here. This observation is expected since the heat propagation via conduction path (1) has a significantly shorter timescale than the overlapping heat dissipation processes related to path 2 and 3.

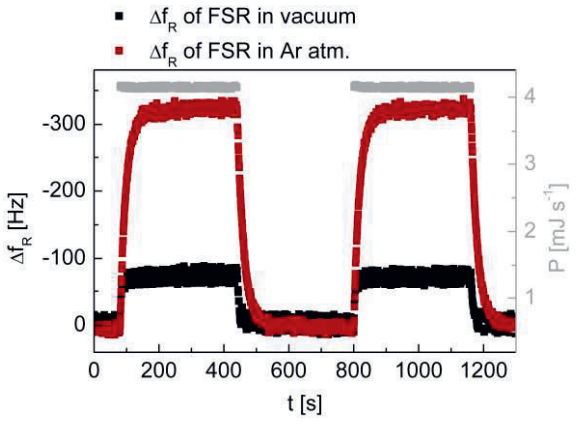

Figure 5: Two cycles of joule heating of FSR in vacuum and argon P = 4.1 mJ s^{-1} for 240 s and subsequent cooling (almost equilibrium condition)

To quantify the total losses of the system at nearly equilibrium conditions, the resonance frequency response to prolonged resistive heating of the vibrating resonator volume is investigated. *Fig.5* presents the resonance frequency for the application of 4.1 mJ s^{-1} over 240 s to the FSR in Argon atmosphere and in vacuum. In presence of the atmosphere the applied energy is partially consumed by the surrounding gas atmosphere. This results in Δf_{R_Ar} = 78 Hz, which is four times smaller than Δf_{R_Vac} = 320 Hz. Prolonged heating reflects clearly losses due to convection. They become significant which is supported by the difference between Δf_{R_Ar} and Δf_{R_Vac} *(Fig. 4)*. Consequently, prolonged PT of a thin film includes convective heat dissipation which must be included in the model of data evaluation. Fitting the heating curve of the vacuum measurement with eq. (6) results in τ_{Vac} = (18.5±0.1 s). This value can be attributed to the radial symmetric heat propagation via heat transfer path (2). In Ar atmosphere the radial symmetric heat propagation occurs simultaneously with heat losses due to convection. Fitting the heating curve with eq. (6) results in the overall heating time constant τ_{Ar} = (5.4±0.4 s). Subsequent cooling data show a uniform cooling of the entire system, resonator shows a uniform temperature distribution at the equilibrium condition after the prolonged heating. Therefore, the cooling curves are fitted with one exponential decay function (eq. 7) with τ_{Vac} = 20.4±0.1 s for vacuum and τ_{Ar} = (5.6±0.3 s) for Argon atmosphere, respectively.

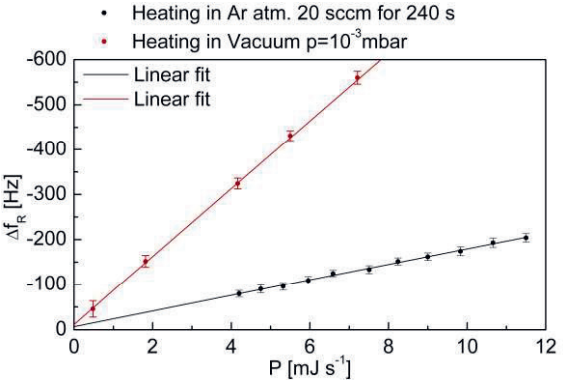

Figure 6: Influence of heating power variation (heating over 240 s almost equilibrium condition at 231.9 °C); standard deviation error bars

Finally, the overall effect of heat dissipation on Δf_R in dependence of the heating power is investigated (*Fig.6*). The latter is varied at 231.9 °C in Ar and vacuum. In both cases a linear dependence of the maximum resonance frequency change on heating power is observed (*Fig. 6*). This behavior is expected for small Δf_R, since the temperature dependence of f_R can be approximated satisfactorily by a linear function for temperature changes <10 K. For larger temperature changes a parabolic dependence of the resonance frequency of the LGS resonators would be observed [14]. Prolonged heating in presence of Ar atmosphere shows significant heat dissipation due to convection. The linear dependence of Δf_R on heating power, exhibits a 4.8 times larger slope in vacuum due to decreased heat transport at the absence of the atmosphere.

The resonator and sample holder arrangement is in nearly equilibrium conditions after prolonged heating which is reached faster in Argon atmosphere. Further, the atmosphere itself causes slight increase in the

total thermal mass to be heated. As a consequence, different slopes for vacuum and argon result.

Summary and Conclusions

A thermodynamic investigation of the TFC system, i.e. of resonator and sample holder, confirms the proposed data evaluation model in [10] for TFC measurements for fast PT. Further, the heat transfer mechanisms are quantified. For short timescales, thermal conduction from a heater structure in this analysis or from a thin film in case of TFC analysis into the vibrating volume of the resonator dominates due to the short timescale of this process. Consequently, conventional resonators and FSR show in Ar atmosphere and in vacuum a nearly identical Δf_R response to short heating pulses. Therefore, for short heating pulses or fast PT of thin films, might be evaluated by ignoring heat radiation and/or convection if an atmosphere is present. Similarly, FSR, which have a reduced thermal conduction path to the vibrating volume, show larger heat dissipation time constants. In general, the use of FSR in vacuum maximizes the time for the determination of the maximum temperature change, induced into the vibrating resonator volume. Thus, the number of measurements is increased. It is therefore advisable to perform TFC measurements on FSR in vacuum for maximized measurement accuracy and minimized losses due to heat dissipation.

Acknowledgments

The authors gratefully thank the German Research Foundation (DFG) for the financial support within the priority program 1473 ‘‘WeNDeLIB’’. Further, the support of the Energie-Forschungszentrum Niedersachsen (EFZN), Goslar, Germany, is acknowledged.

References

[1] Y. K. Sun, S. T. Myung, B. C. Park, J. Prakash, I. Belharouak und K. Amine, High-energy cathode material for long-life and safe lithium batteries, Nature Materials, vol. 8, pp. 320 – 324, 2009.

[2] H. Maleki, S. A. Hallaj, J. R. Selman, R. B. Dinwiddie und H. Wang, Thermal properties of lithium-ion battery and components, Journal of Electrochemical Society, vol. 146, pp. 947–954, 1999.

[3] X. Chen, C. Li, M. Grätzel, R. Kostecki und S. S. Mao, Nanomaterials for renewable energy production and storage, Chemical Society Reviews, vol. 41, pp. 7909–7937, 2012.

[4] P. Balakrishnan, R. Ramesh und T. P. Kumar, Safety mechanisms in lithium-ion batteries, Issue 2 Hrsg., Bd. 155, Journal of Power Sources, 2006, p. 401–414.

[5] M. S. Whittingham, Lithium batteries and cathode materials, Chemical Reviews, vol. 104, pp. 4271–4301, 2004.

[6] R. Sousa, J. F. Riberia, J. A. Sousa, L. M. Goncalves und J. H. Correia, All-solid-state batteries: An overview for bio applications, 2013 IEEE 3rd Portuguese Meeting in Bioengineering (ENBENG), pp. 1–4, 2013.

[7] M. Ohring, Materials Science of Thin Films - Deposition and Structure, Acadeic Press, 2002.

[8] L. Wojtcak, The melting point of thin films, Physica Status Solidi b, pp. K163-K166 1967.

[9] H. Wulfmeier, D. Albrecht, S. Ivanov, J. Fischer, R. Grieseler, P. Schaaf, S. Ulrich, A.Bund, H.Fritze. Thin-film calorimetry -- device development and application to lithium ion battery materials, pp. 16 *MRS Proceedings,* 2012.

[10] H. Wulfmeier, D. Albrecht, S. Ivanov, J. Fischer, S. Ulrich, A. Bund, H. Fritze, High-temperature thin-film calorimerty: A newly developed method applied to lithium ion battery materials, *Journal of Material Science, vol. 48, pp. 6585--6596,* 2013.

[11] H. Wulfmeier, D. Albrecht, J. Fischer, S. Ivanov, a. A. Bund, a. S. Ulrich, H.Fritze, Thin-film calorimetry: Analytical tool for in-situ characterization of lithium ion batteries, *Journal of The Electrochemical Society, vol. 162, pp. A727-A736,* 2015.

[12] H. Wulfmeier, A. Omelcenko, D. Albrecht, D. Klimm, W. El Mofid, M. Strafela, S. Ulrich, A. Bund und H. Fritze, Thermal stability of materials for thin-film electrochemical cells investigated by thin-film calorimetry, *MRS Advances, vol. 1, pp. 1513-1518,* 2016.

[13] H. Fritze, H. L. Tuller, G. Borchardt und T. Fukuda, High-Temperature Properties of Langasite, mrs proceedings, vol 604, pp. 65-71, 2000.

[14] M. Schulz und H. Fritze, Electromechanical properties of langasite resonators, *Journal of Renewable Energy,* vol. 33, pp. 336-341, 2008.

[15] Z.Wang, D.Yuan, L. P. X. Cheng, Y. Lv, X.Wang, S. Guo, X. Duan und J.Wang, Crystal growth and thermal and optical properties of La3Ga5SiO14 single crystals, *Applied Physics A, vol. 254, pp. 264-271,* 2003.

[16] S. Kalpakjian, in *Manufacturing Processes for Engineering Materials*, Pearson Education, Inc., pp. 552–553, 2008.

[17] D. R. Lide, in *Handbook of chemistry and physics*, 84 Hrsg., CRC Press, pp. 15 2003.

[18] R. Ravelo und M. Baskes, Equilibrium and thermodynamic properties of grey, white, and liquid tin, *Physical Review Letters,* Bd. 79, p. 2482–2485, 1997.